Climate Dynamics (2019) 53:4233–4248
https://doi.org/10.1007/s00382-019-04780-7

# Simulated future changes in ENSO dynamics in the framework of the linear recharge oscillator model

**Dietmar Dommenget**[1] · **Asha Vijayeta**[1]

Received: 2 October 2018 / Accepted: 17 April 2019 / Published online: 26 April 2019


**Abstract**
This study analysed the changes in El Niño Southern Oscillation (ENSO) dynamics as they are simulated in 25 models of the CMIP5 simulations for the RCP8.5 scenario relative to the historical control simulation. The ENSO linear recharge oscillator (ReOsc) framework is used to focus on changes in the growth rate of eastern equatorial Pacific sea surface temperature ($T$) and mean equatorial Pacific thermocline depth ($h$) anomalies, the coupling between the two and the noise forcing driving the ENSO variability. We further focused on the feedbacks controlling the growth rate of $T$, namely the Bjerknes wind to sea surface temperature (SST) feedback, the atmospheric net heat flux and the residual oceanic feedback. We find significant changes in nearly all of these important elements of the ENSO dynamics, despite the fact that the ensemble shows very little changes in the overall ENSO variability. The growth rate of $T$ weakens resulting from a combination of increased negative atmospheric net heat flux feedbacks, increased positive Bjerknes wind-SST feedback and increased residual oceanic feedbacks. Further notable changes are, an increase in the growth rate of $h$ and a stronger coupling of $T$ to $h$. Sensitivity analysis of the ReOsc model can explain why these strong dynamical changes lead to effectively no changes in the overall ENSO variability, but are likely to affect the predictability of ENSO.

## 1 Introduction

Anthropogenic climate change not only alters the mean state climate, but also potentially affects the nature of internal climate variability. How in detail the internal variability will change is an important question of anthropogenic climate change research. In particular, the potential changes in the most important mode of natural climate variability, the El Niño Southern Oscillation (ENSO) mode, are still a subject of current research (Collins et al. 2010; Cai et al. 2015b).

Previous studies on changes in the ENSO variability primarily focussed on changes in ENSO statistics, such as the standard deviation (*stdv*) of the sea surface temperature (SST) variability, the power spectral peak of SST (periodicity) or the changes in the pattern of ENSO SST variability (e.g. Van Oldenborgh et al. 2005; Yeh et al. 2009; Collins et al. 2010; Stevenson et al. 2012; Chen et al. 2017). Studies of future climate change with simulations from the couple model intercomparison project (CMIP) found mostly little changes in these statistics. The overall *stdv* of ENSO in the CMIP ensemble mean is not changing significantly and the periodicity of ENSO is also not changing significantly. However, there is large spread in the CMIP ensemble with individual models showing clear trends in these statistics, but with opposing directions, averaging to a near zero ensemble mean result.

A number of studies have analysed changes in recent observed ENSO variability (Lee and McPhaden 2010; McPhaden et al. 2011; McPhaden 2012; Lübbecke and Mcphaden 2014; Guan and McPhaden 2016; Capotondi and Sardeshmukh 2017). These studies suggest that ENSO statistics, dynamics and the pattern have been changing in the recent decades relative to previous decades. A recent study by Zhao et al. (2016) also suggests that the predictability of ENSO is decreasing in recent decades, indicating changes in the dynamics of ENSO. Whether these changes are consistent with the CMIP model projections is, however, unclear. Here it also needs to be considered that changes in observed ENSO characteristics are typically

**Electronic supplementary material** The online version of this article (https://doi.org/10.1007/s00382-019-04780-7) contains supplementary material, which is available to authorized users.

✉ Dietmar Dommenget
dietmar.dommenget@monash.edu

[1] School of Earth, Atmosphere and Environment, Monash University, Clayton, VIC 3800, Australia

based on a relatively short time period, which will make it difficult to distinguish such variations from natural internal low-frequency variability (e.g. Wittenberg et al. 2014).

Much of these observed changes in ENSO are linked to changes in the tropical Pacific mean state (e.g. McPhaden et al. 2011; Zhao et al. 2016). These mean state changes themselves have been analysed in several studies (Liu et al. 2005; Vecchi et al. 2006; Dinezio et al. 2012; England et al. 2014; Bayr et al. 2014; Luo et al. 2015, 2017, 2018; Kohyama et al. 2017). Many of these studies find large differences between observed trends and those project by CMIP simulations. In particular, the changes in the Walker circulation and associated winds, and changes in the equatorial mean SST pattern are inconsistent between recent observations and CMIP model projects. These diverse results are further complicated by the fact the current climate model simulations of ENSO have significant common biases in the underlying processes and dynamics (Bellenger et al. 2014; Vijayeta and Dommenget 2017 hereafter VD18).

Some studies analysed the dynamical changes of ENSO in CMIP3 and CMIP5 model simulations (Kim and Jin 2011; Chen et al. 2015). Both studies analysed heat budget terms of tropical Pacific SST. Kim and Jin (2011) found significant change in elements of ENSO dynamics, that due to competing effects lead to no changes in the stability of ENSO. Chen et al. (2015) explored the dynamical elements that lead to changes in ENSO amplitude. They found that change in the thermocline and zonal advection feedback are the main drivers in ENSO amplitude changes.

The combination of the above-mentioned studies on changes in ENSO variability, we find a fairly diverse picture, with inconsistencies between recent observations and models, between different model simulations and significant model biases in the ENSO dynamics. Given these uncertainties, it is instructive to gain a better dynamical understanding of the changes in the ENSO variability. We therefore focus in this study on the changes in dynamics of the ENSO mode in future climate change simulations.

The analysis of the ENSO dynamics presented in this study will be based on the linear recharge oscillator (ReOsc) model (Jin 1997; Burgers et al. 2005; Jansen et al. 2009). The ReOsc model is a very effective way of describing the essential elements of the ENSO dynamics, such as the SST growth rate and the coupling to the SST to the thermocline depth, which represents the delayed negative feedback leading to the observed oscillating nature of ENSO. It can be used as an effective diagnostic tool to estimate these important dynamical elements of ENSO based on the outputs of model simulations or observations. It can further be used to understand how changes in important dynamical aspects, such as the wind-SST feedback affect ENSO statistics. VD18 has illustrated in a recent study that the ReOsc model describes the ENSO dynamics and statistics in the diverse CMIP ensembles very well.

This study is organized as follows: the next section introduces the CMIP model data, the ReOsc model equations and how it is used to estimate the ENSO dynamics. It also discusses some of the limitations in this approach. Section 3 presents the main results of this study, starting with analysis of the thermocline depth, some simple ENSO statistics followed by an analysis of the ReOsc dynamics, which is the main focus of this study. The section will be concluded with a look at possible changes in the predictability. The last section provides a summary and discussion.

## 2 Data, models and methods

### 2.1 CMIP5 model simulations

The analysis is based on CMIP5 model simulation of the historical and the RCP8.5 scenario (Moss et al. 2010; Taylor et al. 2012). We use all model simulations that have all variables available needed for this analysis. These are 25 model simulations, see Table 1. The historical scenario over the period from 1881 to 1980 is considered as the control climate. The RCP8.5 from 2051 to 2100 is considered for the climate change period. All data is linearly detrended and anomalies relative to the mean seasonal cycle are defined.

### 2.2 The recharge oscillator model

The linear ENSO dynamics are evaluated on the basis of the ReOsc model from Burgers et al. (2005), Frauen and Dommenget (2010) and VD18. This model is given by two tendency equations of the NINO3 region (150°W–90°W, 5°S–5°N) SST anomalies, $T$, and equatorial Pacific (130°E–80°W, 5°S–5°N) mean thermocline depth anomalies, $h$:

$$\begin{aligned} \frac{dT(t)}{dt} &= a_{11}T(t) + a_{12}h(t) + \zeta_T \\ \frac{dh(t)}{dt} &= a_{21}T(t) + a_{22}h(t) + \zeta_h. \end{aligned} \tag{1}$$

The model parameters $a_{11}$ and $a_{22}$ represent the growth rate (or damping) of $T$ and $h$, and the parameters $a_{12}$ and $a_{21}$ the coupling between $T$ and $h$. The two equations are forced by stochastic noise terms $\zeta_T$ and $\zeta_h$. The parameters of the 2-dimensinal model Eq. (1) are estimated for each CMIP5 model simulation by multivariate linear regression the monthly mean tendencies of $T$ and $h$ against monthly mean $T$ and $h$, respectively, following the approach in previous studies (Burgers et al. 2005; Jansen et al. 2009 and VD18).

**Table 1** List of CMIP5 models used in this study

| Model |
|---|
| 1. ACCESS1-0 |
| 2. ACCESS1-3 |
| 3. BNU-ESM |
| 4. CESM1-BGC |
| 5. CESM1-CAM5 |
| 6. CMCC-CM |
| 7. CNRM-CM5 |
| 8. CSIRO-Mk3-6-0 |
| 9. CanESM2 |
| 10. GFDL-CM3 |
| 11. GFDL-ESM2G |
| 12. GFDL-ESM2M |
| 13. GISS-E2-H-CC |
| 14. GISS-E2-H |
| 15. GISS-E2-R-CC |
| 16. GISS-E2-R |
| 17. IPSL-CM5A-LR |
| 18. IPSL-CM5A-MR |
| 19. IPSL-CM5B-LR |
| 20. MIROC-ESM-CHEM |
| 21. MIROC-ESM |
| 22. MIROC5 |
| 23. MRI-CGCM3 |
| 24. NorESM1-ME |
| 25. bcc-csm1-1 |

The numbers in this table refer to the numbers used in the figures

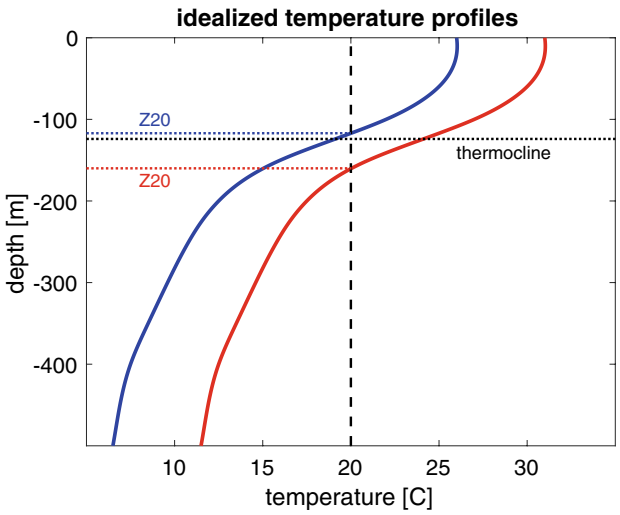


**Fig. 1** Sketch of idealised temperature profiles, *Z20* and thermocline depth (*maxgrad*). The blue and red temperature profiles are identical with the only difference of a constant off set of 3 °C. The thermocline depth is the same for both profiles, but Z20 is deeper in the warmer profile

The ReOsc model approach is different from the widely used Bjerknes stability (BJ) index or similar SST heat budget analysis (e.g. Jin et al. 2006; Kim and Jin 2011; Kim et al. 2014; Chen et al. 2015). The terms of the BJ-index analysis can in most cases not be directly related to the parameters of the ReOsc, and it only discusses SST stability. In turn, the advantage of the ReOsc model is that the dynamical parameters of the model can be more directly linked to the ENSO variability statistics, such as standard deviation (*stdv*) of *T*, *stdv*(*h*), the power spectrum or coupling between T and h, by integrating the ReOsc model equations (VD18).

The residual of the linear regression fit for the ReOsc model can be interpreted, as the random noise forcings with the *stdv* of the residuals being the *stdv* of the noise forcings for the *T* and *h* equations ($\zeta_T$ and $\zeta_h$). However, it also needs to be considered that this simple linear model fit does not fully represent the ENSO dynamics in the models. Mismatches between the true, more complex, dynamics and the ReOsc model fit will also project onto the residual noise terms of the model. VB18 did evaluate the goodness of fit to the CMIP model. They found that the residual noise terms fit well with the white noise assumption, but they also do show some indications of the linear ReOsc model does not fully represents the ENSO dynamics in the CMIP models, leading to some enhanced spread in the noise terms.

The thermocline depth (h) marks the depth at which the vertical temperature gradients are largest, see sketch in Fig. 1. It is often estimated on the basis of the depth of 20 °C isotherm (*Z20*), because this is a more robust approximation when the data is of coarse resolution (Meyers 1979; Kessler 1990; Smith 1995; Yang and Wang 2009). Studies of future climate change simulations often used the maximum in the temperature gradients to estimate the thermocline depth (Vecchi and Soden 2007; Yeh et al. 2009). Previous studies with the ReOsc model used *Z20* to estimate the thermocline depth (h) (Burgers et al. 2005; Jansen et al. 2009 and VD18).

However, this poses a problem when studying climate change, because a uniformly warming temperature profile will not change the thermocline depth, but will lead to deeper *Z20* (Yang and Wang 2009), see sketch in Fig. 1. This may potentially lead to artificial changes in the ReOsc model dynamics, even though nothing may have changed in the dynamics. To address this problem, we evaluate the ENSO dynamics and the ReOsc model parameters on the basis of both, a *Z20* and a maximum gradient (*maxgrad*) estimate of the thermocline. Both estimates are based on high-resolution (0.1 m) spline fits of the CMIP5 simulation temperature profiles. In the following analysis, we will use the *maxgrad* estimate for the thermocline depth if not otherwise noted.

The growth rate of *T* ($a_{11}$) in the ReOsc model can be split into an atmospheric ($a_{11A}$) and oceanic contribution

($a_{11O}$) following the approach of (Frauen and Dommenget 2010 and VD18):

$$a_{11} = a_{11A} + a_{11O}. \quad (2)$$

The atmospheric growth rate of $T$ ($a_{11A}$) is estimated as a linear combination of atmospheric heat flux feedback ($c_{fT}$), the wind-stress (Bjerknes) feedback ($c_{\tau T}$):

$$a_{11A} = a_{12}\lambda C_{\tau T} + \frac{C_{fT}}{\gamma}. \quad (3)$$

$c_{\tau T}$ is the linear regression of zonal wind stress, $\tau_x$, in the central Pacific region (160°E–140°W, 6°S–6°N) and $T$, and $c_{fT}$ is the linear regression of net atmospheric heat flux in the NINO3 region and $T$. λ is a positive free coupling parameter and $\gamma$ the ocean mixed layer depth that are assumed to be constant for all simulations (VD18). $a_{11O}$ is estimated as the residual growth rate:

$$a_{11O} = a_{11} - a_{11A}. \quad (4)$$

VD18 provided a proof of concept, illustrating this ReOsc model approach. They found, for instance, that the ReOsc model is capable in reproducing the CMIP model simulations *stdv*($T$) with correlation of 0.99 by integrating Eq. (1) with the estimated model parameters. Similarly, other important statistics, such as *stdv*($h$), the cross correlation between T and h or the power spectral slope (see section below for a definition) are also reproduced very well (correlation > 0.8) with this approach.

However, the model does have some limitations and it does make some simplifications. Some notable limitations are, as discussed in VD18: The power spectral distribution of variance is wider in the CMIP model simulations than it is simulated in the ReOsc fitted to the CMIP models. The cross-correlation between T and h is slightly overestimated in the fitted ReOsc models, and, as mentioned above, the residual noise forcing terms are not just white noise forcings, but do partly reflect more complex dynamics that are not captured by this linear ReOsc model approach.

Important simplifications of the ReOsc model: It is a linear approach and therefore does not consider non-linearity in the ENSO dynamics or state dependent noise forcings. Further, the model describes ENSO in a one-dimensional SST index (T), therefore neglecting ENSO diversity in respect to regional differences in the ENSO amplitudes (e.g., central Pacific vs. east Pacific events).

### 2.3 Estimation of sensitivities with the recharge oscillator model

The sensitivity of ENSO statistics to changes in the ReOsc model parameters can be estimated by integrating the ReOsc model with white noise forcing (see also VD18). We therefore integrate the ReOsc model for 1000 years with all parameters set to the mean values of the historical simulations. Based on the resulting $T$ and $h$ time series we compute the control ENSO statistics. In a second integration, we use the same white noise forcings, but change one or all of the ReOsc model parameters to the mean values of the RCP8.5 simulations. Based on the resulting $T$ and $h$ time series we compute the RCP8.5 ENSO statistics, and the differences to the control simulations provides us an estimate of the sensitivity to the parameter changes. Given that we used the same white noise forcings in both integrations, these estimates have no statistical uncertainties from the integrations.

### 2.4 The power spectral slope

The spectral power slope is a non-dimensional characteristic of a power spectrum that effectively captures the time scale behaviour. Following the approach of VD18 we estimated the slope (in log-scale) from 1 to 7 years period to capture the range of the power spectrum in which the variance is strongly increasing with period (decreasing with frequency) and where the ENSO variance peaks. Simulations with a more pronounced interannual peak tend to have steeper slopes (more negative), and those with a less pronounce interannual peak or a shift towards low-frequencies tend to have a less steep slope (less negative). The spectral power slope therefore captures changes in the time scale behaviour or periodicity relatively well. This is in particular true for a damped oscillation as described by the ReOsc model.

We tested this approach in a wide range of different CMIP simulations and ReOsc models (Eq. 1) integrated with different parameters and found this metric to be the best fit to describe variations of the peak of the power spectrum. An increased (less step or more flat) slope in these simulations corresponds, in statistical average, to a shift in the peak towards lower frequencies. In turn, a decreased (stepper or less flat) corresponds, in statistical average, to a shift in the peak towards higher frequencies. However, it needs to be noted that it is only one parameter describing a power spectrum that has more than one degree of freedom. Therefore, changes in the power spectrum can occur that are no capture by this parameter.

### 2.5 Estimates of uncertainties

In the following analysis, we will estimate uncertainties in the ENSO statistics and the ReOsc model parameters in two ways: First, we will provide a confidence interval for the statistical significance in changes from the historical to the RCP8.5 simulation for each individual model. Second, we will provide a confidence interval for changes in the ensemble mean values.

The 95% confidence interval for all parameters based on regressions (e.g., ReOsc model parameters and power

spectral slope), are estimated for each individual model for the 50 years period of the RCP8.5 simulations. However, instead of presenting the confidence interval for each individual simulation we only show the mean 95% confidence interval of the ensemble in reference to the one-to-one line (e.g. see Figs. 5, 6, 7). This effectively illustrates if individual model parameters have changed from the historical to the RCP8.5 simulations. For uncertainties in the standard deviations, we followed a Chi squared distribution approach and assumed that the confidence interval is proportional to the expectation value (e.g. see Fig. 5a). The ensemble mean uncertainties are presented by 95% confidence interval of a Students *t* test, assuming that each simulation represents an independent sample (e.g., see red line in Fig. 5a).

## 3 Results

### 3.1 Thermocline depth changes

The thermocline depth is one of the two dynamical variables of the ReOsc model, representing a proxy of upper ocean heat content. Mean state changes in the thermocline depth can affect the dynamics of ENSO, but potentially will also affect the estimation of the thermocline depth by *Z20* (see sketch in Fig. 1). It is therefore a good starting point for the analysis of the dynamical changes of ENSO.

Figure 2 shows the mean temperature profiles of the equatorial Pacific for the historical and RCP8.5 CMIP5 ensemble mean together with thermocline depth estimates. The temperature profile warms on all levels, but the warming is not uniform with depth, see Fig. 2b. The strongest warming is at the surface and the least amount of warming is very close to the mean thermocline depth of the historical simulations, followed by stronger warming in deeper layers. This profile is very different from what may have been expected from a transient or equilibrium warming (e.g. Manabe et al. 1991; Rhein et al. 2013; Yoshimori et al. 2016) It suggests a dynamical adjustment of the upper equatorial Pacific, which leads to reduced warming at the thermocline depth.

The thermocline depth becomes shallower in the RCP85 scenario, which is due to the fast warming at the surface layers. This is consistent with the results of previous studies of simulated future thermocline depth changes (Vecchi and Soden 2007; Yeh et al. 2009; Kim and Jin 2011; Chen et al. 2015). In turn, *Z20* does deepen, but not as much as one may have expected from a homogenous warming. This is due to the minimum of warming at the thermocline, which counteracts the deepening of *Z20*.

The different behaviour of the thermocline depth and *Z20* is also reflected in the regional changes of the equatorial Pacific, see Fig. 3. The thermocline depth decreases relatively uniformly, but more in the central and west Pacific, and less in the east Pacific. *Z20* shows a fairly different behaviour. It strongly deepens in the eastern Pacific and slightly along the equator. Off the equator *Z20* becomes shallower, in contrast to what you would expect from a warming temperature profile. Upper layers (above *Z20*) of the off-equatorial central Pacific cool (not shown), leading to a shallowing of *Z20*. This suggests a strong dynamical rearrangement of the upper equatorial Pacific: warm upper ocean off-equatorial water shifts into the equatorial region.

These changes in the thermocline depth also affect the cross-correlation between *T* and *h* (Fig. 4). In the historical CMIP5 simulations *T* and *h*(*Z20*) have a very clear out-of-phase relation, with a strong positive correlation when *h* leads *T* and a roughly equally strong negative correlation when *T* leads *h* at about the same lead time of 5–8 months

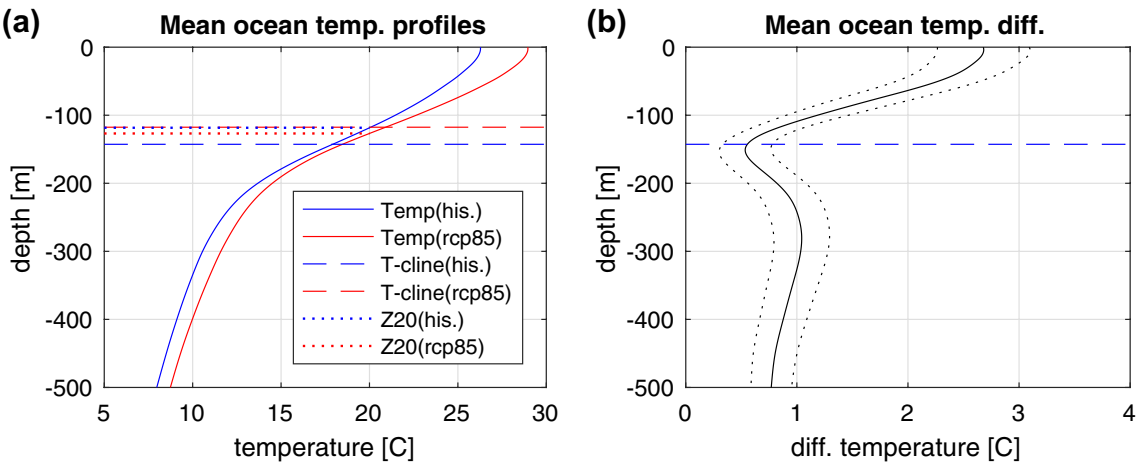


**Fig. 2** **a** CMIP5 equatorial Pacific mean (150°E–80°W, 5°S–5°N) temperature profiles of the historical (blue) and RCP8.5 (red) scenario. Estimates of the thermocline depth (*maxgrad*) and *Z20* are shown as well. **b** Difference in the temperature profiles. The dotted lines mark the 95% confidence interval

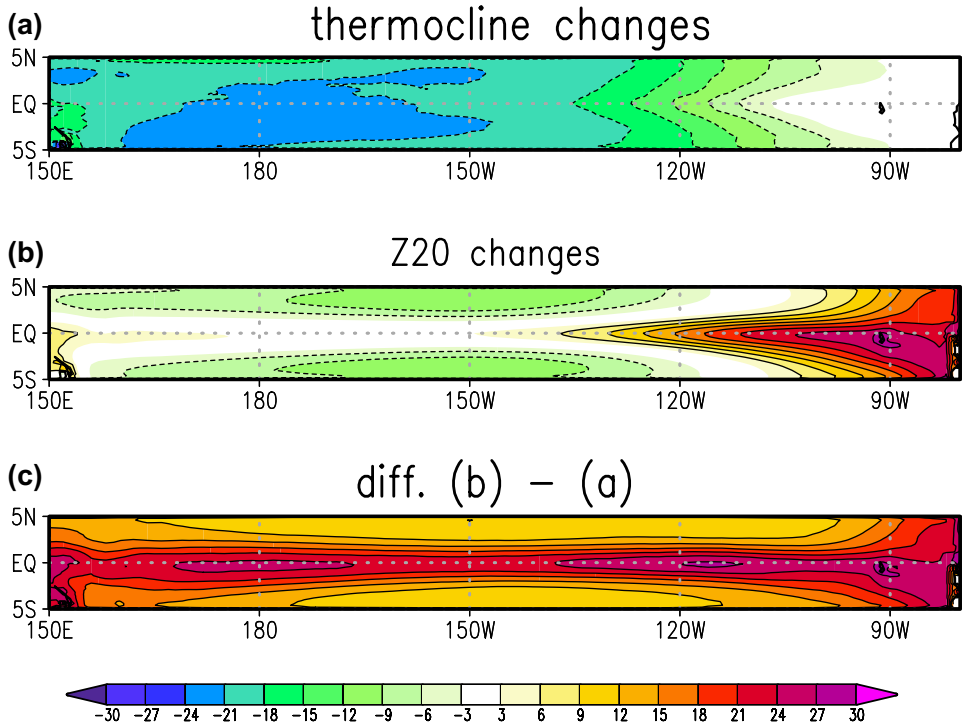


**Fig. 3** Mean changes in **a** the thermocline depth (*maxgrad*) and **b** *Z20* for CMIP RCP8.5 minus historical simulations over the equatorial Pacific domain. **c** Is the difference of **b**–**a**. Negative values indicate shallower thermocline depth in the RCP8.5 simulations. Values are in m

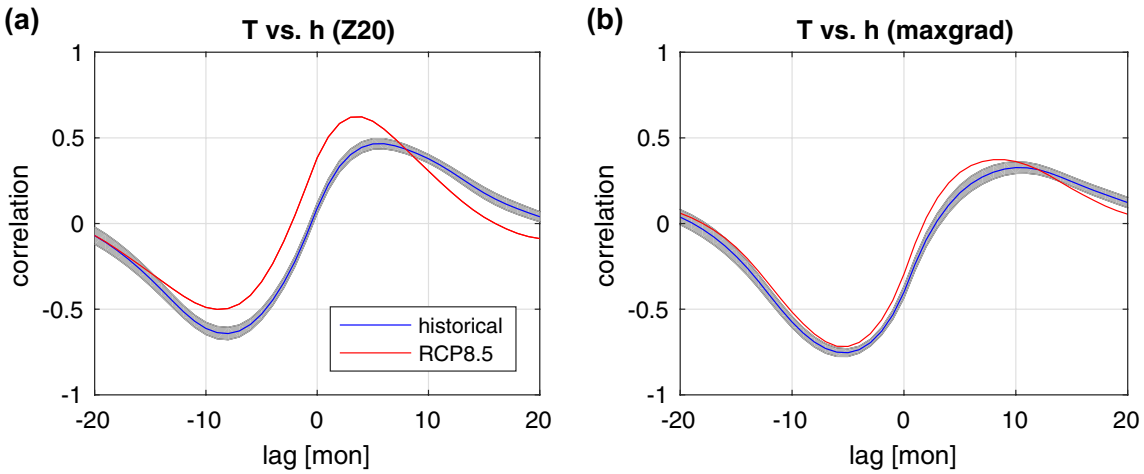


**Fig. 4** The cross-correlation of *T* vs. *h* for **a** the *Z20* and **b** the *maxgrad* estimates. The blue lines are the historical ensemble mean values and the grey shaded area mark the standard error for a t-test. The red lines are the RCP8.5 ensemble mean values. Positive lag times indicate the time evolution of *h* leads *T*

(Fig. 4a). This does change significantly in the future RCP8.5 simulations for *Z20* estimates. The cross-correlation shifts upwards between the lags −12 to +8 months, leading to a now significant positive instantaneous (lag = 0) correlation (Fig. 4a). It further leads to a change of the peak cross-correlation at positive lead times, with a shift to smaller lead times and an overall increase in correlation at the peak.

These changes are qualitatively similar in the *maxgrad* estimates, but are much weaker. A notable difference to the *Z20* estimate can be seen in the mean cross-correlation of the historical simulations. The *maxgrad* estimates has a quite significant negative instantaneous (lag = 0) cross-correlation and the cross-correlation peak for negative lead times (T leads h) is much larger than the one for positive lead times.

The different characteristics of the thermocline depth estimates as discussed in this subsection indicate that they can potentially affect the ReOsc model parameters and therefore the dynamics of ENSO as estimates by the ReOsc model.

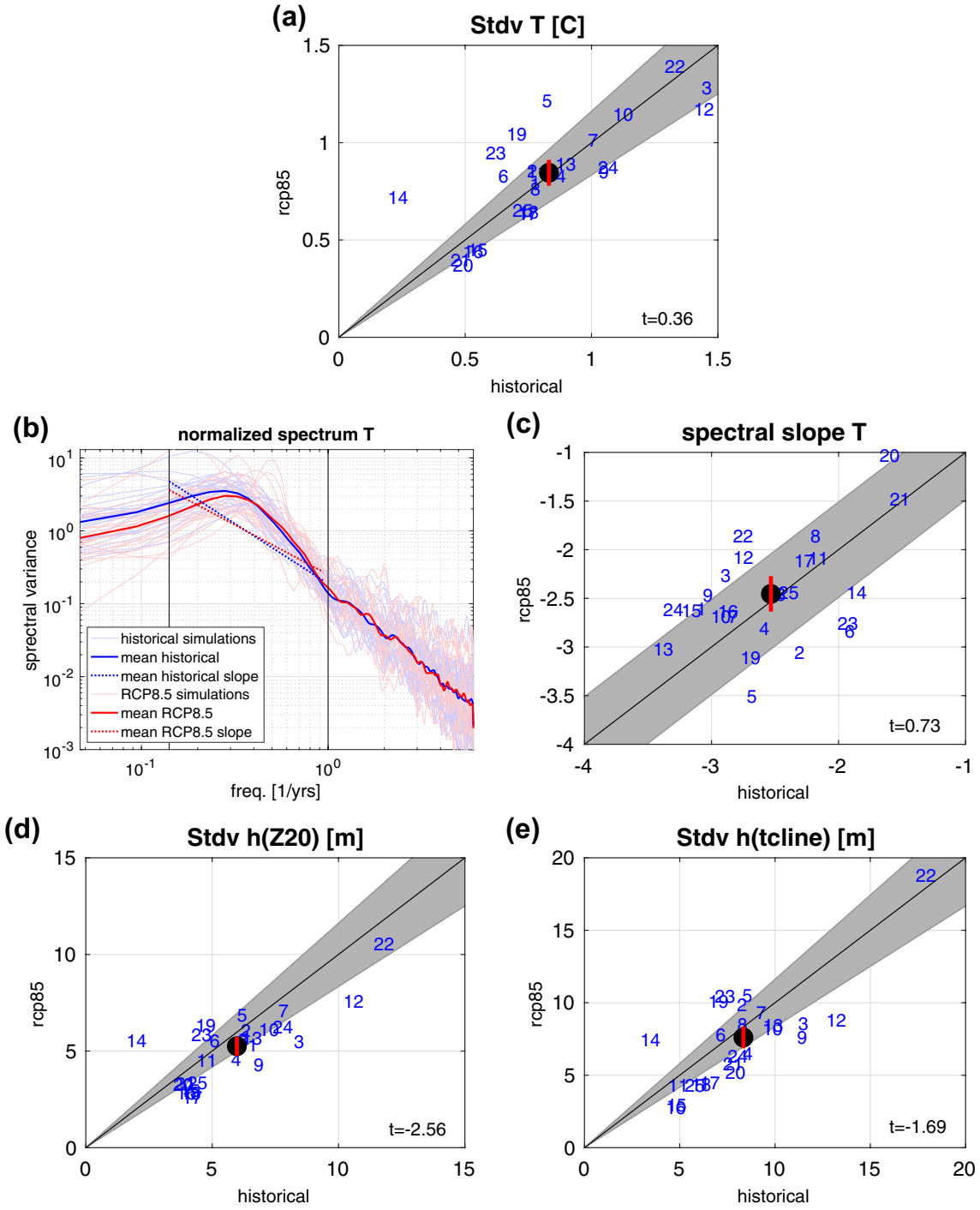


**Fig. 5** Statistics of ENSO variability: **a** *stdv*(*T*), **b** power spectrum of T normalized by the mean variance within 7–1 years period, **c** power spectral slope of *T* variability, **d** *stdv*(*h*) for the *Z20* estimate and **e** *stdv*(*h*) for the *maxgrad* estimate. Each blue number marks a different model (see Table 1). Ensemble mean values in **a**, **c**, **d** and **e** are marked by the black circle with the red line marking the 95% confidence interval. The shaded area around the one-to-one line in **a**, **c**, **d** and **e** mark the mean 95% confidence interval for the individual models (see Sect. 2 for details). The t values for the ensemble mean differences are shown in lower left corner of **a**, **c**, **d** and **e**. An absolute t value $>2.0$ passes the 95% confidence interval. Supplemental Table S1 lists all model values shown in **a**, **c**, **d** and **e**. The two black vertical lines in **b** mark the frequency interval over which the spectral slopes have been estimated

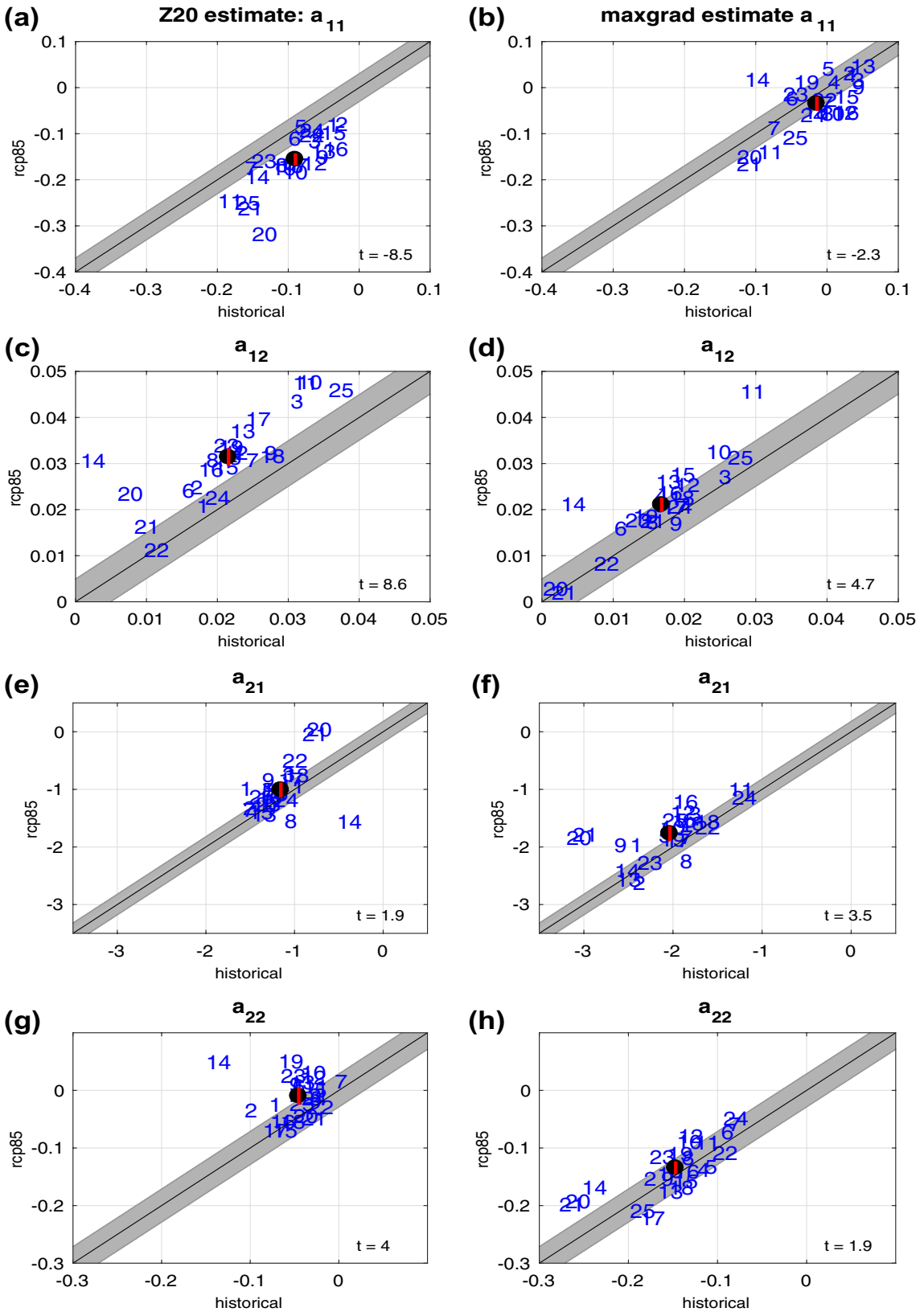


**Fig. 6** ReOsc model parameters: left column for the *Z20* estimate and right column for the *maxgrad* estimates. Growth rate of $T$ ($a_{11}$; upper row), coupling of $T$ to $h$ ($a_{12}$; second row from top), coupling of $h$ to $T$ ($a_{21}$; third row from top) and growth rate of $h$ ($a_{11}$; lowest row). Details as in Fig. 5. Supplemental Table S2–3 lists all model values shown in this figure

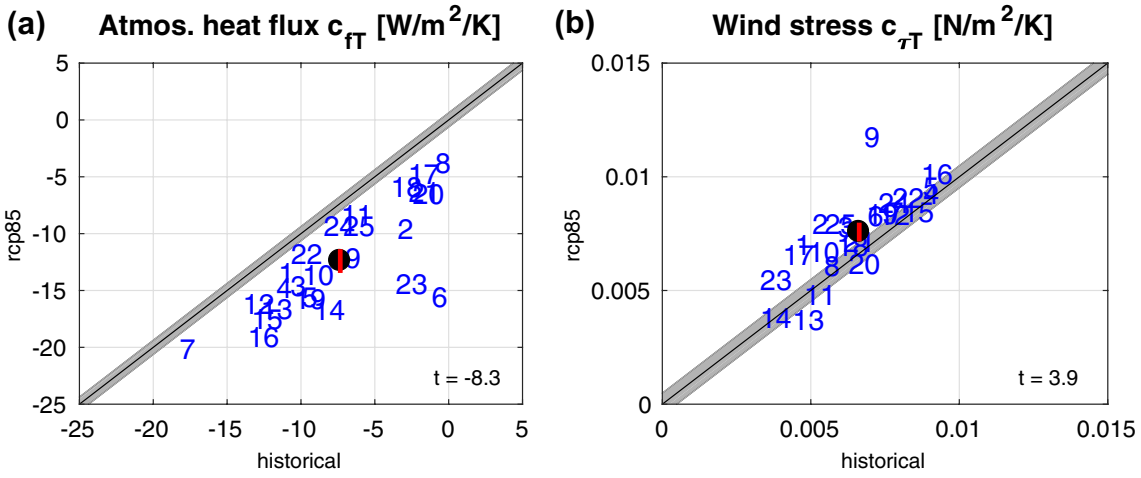


**Fig. 7** **a** Atmospheric net heat flux feedback ($c_{fT}$) and **b** wind-stress feedback ($c_{\tau T}$). Details as in Fig. 5. Supplemental Table S4 lists all model values shown in this figure

We will therefore, in the following analysis section, consider both thermocline estimates.

### 3.2 Changes in statistics of ENSO variability

Before we start analysing changes in the ENSO dynamics, it is instructive to look at changes in the overall statistics of ENSO variability. Similar analysis has been done in previous studies, and we therefore will keep this discussion short to focus more on the dynamical changes.

Figure 5 shows statistics of $T$ and $h$ variability. In addition to the standard deviation of T, Z20 and the thermocline depth, an estimate of the spectral power of T and its slope is shown (see Sect. 2 for details). The standard deviation of $T$ (Fig. 5a) is essentially unchanged in most models. However, some models do show quite significant changes (e.g., models 14 or 5).

The power spectrum of T varies from model to model, but the historical and RCP8.5 scenario spectra are nearly identical in ensemble mean, with some reduction in variance on the lower frequencies in the RCP8.5 scenario (Fig. 5b). The reduction in decadal variability in the RCP8.5 scenario may be related to the missing external forcings such as volcanoes or variations in aerosols (Maher et al. 2014). The reduction in decadal variance is reflected in slightly, but statistically not significant, flatter slope in the interannual variability (see Fig. 5b, c). This suggests no significant change in the periodicity of ENSO is present in the CMIP5 simulations. Some models, however, do show some changes in opposite directions (e.g., models 5 and 22; Fig. 5c).

The standard deviation of $h$ slightly decreases for both, the *Z20* and the *maxgrad* estimates. Indeed, the changes in standard deviation of $h$ highly correlate within the CMIP5 ensemble (correlation 0.9 between the *Z20* and *maxgrad* estimates). However, the changes are more significant in the *Z20* estimate. Overall, the variability statistics show very little changes, neither in the ensemble mean nor for most individual models. Despite missing changes in the ENSO statistics, we cannot conclude that the dynamics of ENSO have not changed, as we will illustrate in the following subsections.

### 3.3 Changes in the recharge oscillator dynamics

The ReOsc model parameters give a good first guess estimate of the linear ENSO dynamics. Thus, changes in these dynamics provide a good first guess of changes in the linear ENSO dynamics. Figure 6 shows the ReOsc model parameters and how they change for both thermocline depth estimates (*Z20* and maxgrad). A comparison of the *Z20* and *maxgrad* estimates of the ReOsc model highlights some significant difference in the mean parameters (see Fig. 6 left vs. right column). In the historical simulations, the *Z20* estimates of the ReOsc model finds a negative growth rate (damping; $a_{11}$) for all models, whereas the *maxgrad* estimates finds values centred around zero. Somewhat the opposite holds for the growth rates of $h$. It is beyond the scope of this study to further explore these differences in the mean ENSO dynamics resulting from the *Z20* and *maxgrad* estimates. However, future studies should address the implications of such differences for the understanding of ENSO dynamics and the role of the thermocline estimates.

Focussing on the changes in the parameters, we can find a significant decrease in the growth rate of $T$ ($a_{11}$; Fig. 6a, b). This is more strongly so in the *Z20* estimate, but still present in the maxgrad estimates too. In the *Z20* estimates it decreases in every single model simulation, which for most models suggest an increase in the damping (negative

growth rate) of T by more than a 100%. This is most striking considering that increased damping of $T$ should reduce $stdv(T)$, but this is not simulated in the CMIP5 simulations (Fig. 5a). This apparent mismatch will be discussed further in Sect. 2.4, when we discuss the sensitivity of the ENSO statistics to the dynamical changes.

The coupling of $T$ to $h$ ($a_{12}$; Fig. 6c, d) increases significantly in nearly all models and in the ensemble mean. This indicates that $T$ is becoming more sensitive to variations in $h$. This may be a reflection of the shallower and more pronounced thermocline depth (maxgrad) in the RCP85 scenario (Fig. 2a). In turn, the coupling of $h$ to $T$ ($a_{21}$; Fig. 6e, f) also increases slightly. However, this change suggests that $h$ is becoming less sensitive to $T$, since $a_{21}$ is negative. This change is more pronounced in the *maxgrad* estimate of $h$. The growth rate of $h$ ($a_{22}$; Fig. 6c, d) increases significantly for the *Z20* estimates and slightly, but not statistically significant, for the maxgrad estimates. This increase in growth rate would suggest an increase in $stdv(h)$, but the CMIP5 simulations show a small decrease (Fig. 5c, d).

In addition, to the ReOsc model parameters, the strength of the noise forcings can change [$\zeta_T$ and $\zeta_h$ in Eq. (1)]. However, changes in $stdv(\zeta_T)$ and $stdv(\zeta_h)$ are small and not statistically significant (not shown). The changes in both $stdv(\zeta_T)$ and $stdv(\zeta_h)$, even though not strong, are highly correlated (0.9) in the CMIP5 ensemble members between the *Z20* and *maxgrad* estimates. This suggest that changes in the forcing strength of *Z20* and the thermocline (*maxgrad*) behave similarly.

The growth rate of $T$ ($a_{11}$) can be split into a number of atmospheric and ocean processes to further gain insight in the changes of ENSO dynamics [see Eqs. (2–4)]. The atmospheric feedbacks are a combination of the net heat flux feedback ($c_{fT}$) and the wind-stress (Bjerknes) feedback ($c_{\tau T}$). Both of these feedbacks show significant changes, see Fig. 7. The atmospheric net heat flux feedback becomes more negative in every single model simulation with an average increase in the negative feedback for each model by a factor of 3 (Fig. 7). The change in $c_{fT}$ is consistent with the increased overall damping of $T$ ($a_{11}$). This change in $c_{fT}$ is consistent with the increased thermodynamical damping in the BJ-index analysis of Kim and Jin (2011). The Bjerknes feedback ($c_{\tau T}$) increases slightly (~ 15%), but still statistically significant. This increase counteracts the increased overall damping of $T$ ($a_{11}$).

The combined contribution of $c_{fT}$ and $c_{\tau T}$ to the overall damping of $T$ ($a_{11}$) can be summarized to an atmospheric damping of T ($a_{11a}$) and the residual contribution to $a_{11}$ as an oceanic feedback [$a_{11o}$; see Eq. (4)]. Figure 8 shows the distribution of $a_{11}$ and $a_{11o}$ in the historical and RCP8.5 scenario simulations. The atmospheric feedbacks ($a_{11a}$) are positive in all model simulations and become even more so in the RCP8.5 scenario. The increase in $a_{11a}$ illustrates that the slight increase in $c_{\tau T}$ overcompensates the decrease in $c_{fT}$. Similarly, but with revised sign, the oceanic feedbacks ($a_{11o}$) are negative in all model simulations and become even more so in the RCP8.5 scenario, which, combined with the changes in $a_{11a}$, gives a shift in the distribution to the upper left in Fig. 8. The overall increased damping of $T$ ($a_{11}$) is a combination of increased ocean and atmospheric net heat flux damping and counteracting increased positive Bjerknes feedback.

In summary, we found stronger and more significant changes in the ENSO dynamics (Figs. 4, 6, 7, 8) than in

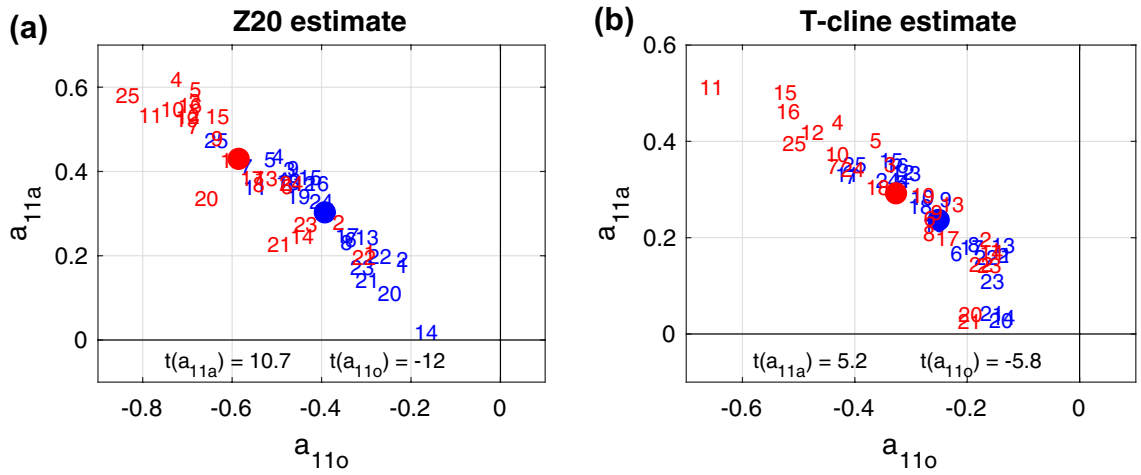


**Fig. 8** Atmospheric ($a_{11A}$) and oceanic ($a_{11o}$) contributions to the growth rate of $T$ for **a** the *Z20* and **b** *maxgrad* estimates. Historical ensemble mean values are marked by the blue circles and RCP8.5 values in red circles. The t values for the ensemble mean differences are shown in upper right corners of each panel. An absolute t value > 2.0 passes the 95% confidence interval. Supplemental Table S4 lists all model values shown in this figure

the statistics of the ENSO variability (Fig. 5). All of these dynamical changes are qualitatively similar in the *Z20* and *maxgrad* estimates of *h*, but in most of them are more pronounced in the *Z20* estimates. The qualitative agreement in the *Z20* and *maxgrad* estimates suggests that these results are robust, independent of how the thermocline depth variability (h) is estimated. The significant changes in the dynamics in the absence of equally significant changes in the statistics of the ENSO variability suggests that the changes in the dynamics must have counteracting effects on the ENSO variability. This will be explored further in the following subsection.

### 3.4 Sensitivity of ENSO variability to the changes in the dynamics

We can use the ReOsc model to evaluate how the changes in the ENSO dynamics would affect the ENSO variability (see Sect. 2 for details). Figure 9 shows the sensitivities for *stdv*(*T*), *stdv*(*h*), the slope of the *T* power spectrum and the cross-correlation between *T* and *h*. Here we focus on the *Z20* estimates and do not discuss the *maxgrad* estimates, as they are qualitatively similar.

We can first of all note that the changes in the statistics of the ENSO variability in the CMIP5 simulations are very well captured by the integrations of the ReOsc model with changes in the parameters, for all four statistics of the ENSO variability (compare CMIP5 with *all* in Fig. 9a–c). Thus, the ReOsc model is a good approximation of how these changes in ENSO statistics relate to changes in the ENSO dynamics.

The sensitivity to the individual ReOsc parameters shows some clear counteracting effects for the different ENSO statistics. The *stdv*(*T*) has overall very little change, resulting from a compensation of decreased variability due to the increased damping of *T* ($a_{11}$) and an increased variability due to the decreased damping of *h* ($a_{22}$; Fig. 9a). The *stdv*(*h*)

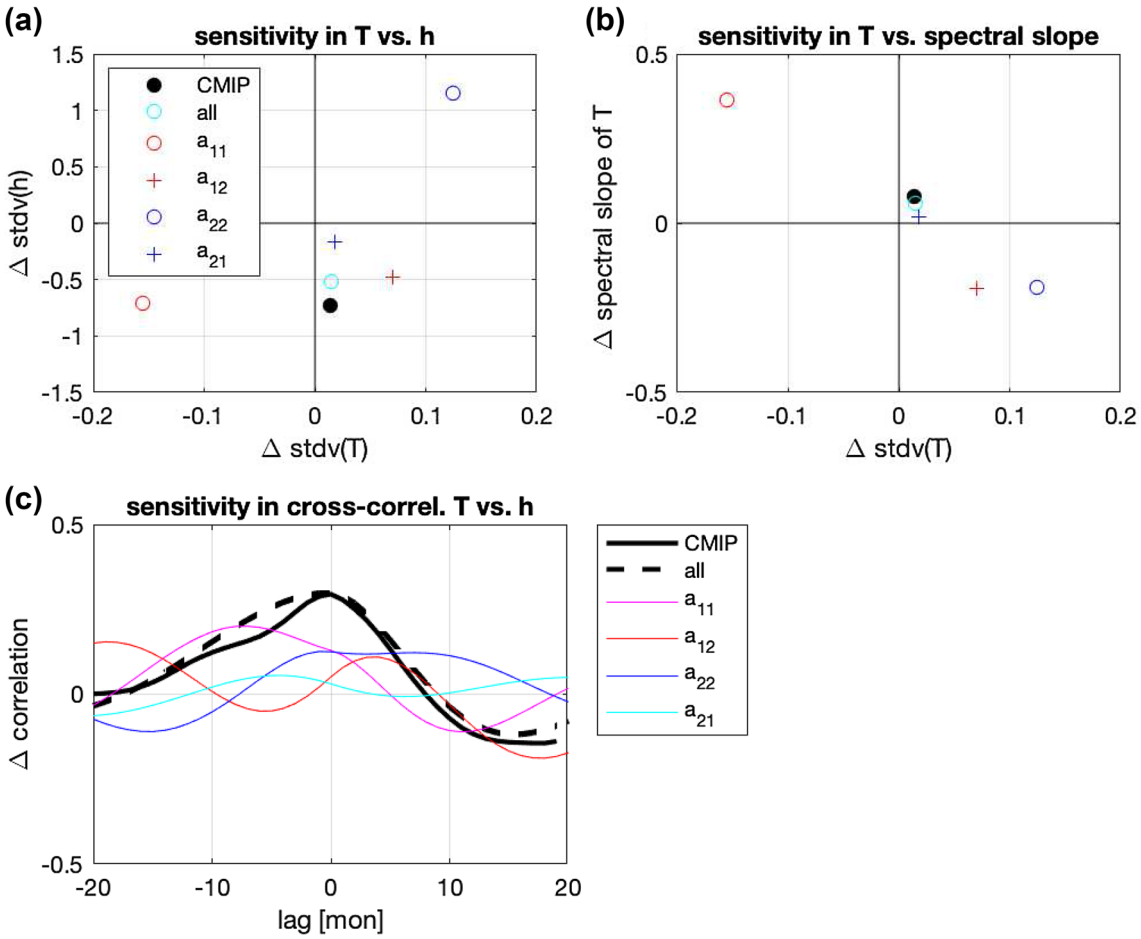


**Fig. 9** Changes in statistics of ENSO variability due to changes in the ReOsc parameters: **a** differences in *stdv*(*T*) vs. *stdv*(*h*), **b** differences in *stdv*(*T*) vs. spectral slope of *T* and **c** the differences in cross-correlation of *T* vs. *h*. CMIP5 model ensemble mean changes are marked by "CMIP" and changes in the ReOsc model integrations due to changes in one or all parameters are marked by the coloured markers or lines. Positive changes in all statistics imply larger values in the RCP8.5 simulations relative to the historical. Positive lag times in **c** indicate the time evolution of *h* leads *T*

behaves similarly, but with opposite signs for sensitivities in $a_{11}$ and $a_{22}$. In addition, the increased coupling of $T$ to $h$ and, to a lesser extent, the decreased coupling of $h$ to $T$ reduces the variability in $h$ (Fig. 9a).

The sensitivity of the power spectral slope of $T$ variability is anti-correlated to the sensitivity of $stdv(T)$ (Fig. 9b), suggesting that increased $T$ variability goes along with a more strongly negative slope in the power spectrum of $T$. The latter is, in statistical average, an indication of a more pronounced interannual variability (peak). Subsequently, the decreased damping of $h$ increased the interannual variability (peak), and in turn the increased damping of $T$ decreased it, combined leading to essentially no change in the power spectral slope.

The cross-correlation between $T$ and $h$ is mostly shifting upwards between the lags $-10$ to $+8$ months (Fig. 4a). This difference in cross-correlation is well captured by the ReOsc model integration (Fig. 9c). It results from a combination of changes in mostly $a_{11}$ and $a_{22}$. The increased damping in $T$ essentially reduces the cross-correlation between $T$ and $h$, since the changes (Fig. 9c) are roughly the opposite of the mean cross-correlation (Fig. 4a). The decreased damping in $h$ is somewhat opposing the effect of increased damping in $T$ for longer lag/lead times. However, the instantaneous (lag = 0) correlation is increased by both changes in $a_{11}$ and $a_{22}$. This results in the future RCP8.5 cross-correlation being now much more in-phase, rather than a clear out-of-phase relation.

The changes in the coupling of $T$ to $h$ have a somewhat weaker, but still relevant impact on the cross-correlation. They show a somewhat higher frequency oscillation (red line in Fig. 9c) than the overall cross-correlation (Fig. 4a) with the same signs for shorter lag/lead times as the overall cross-correlation. This suggests a shift of the peaks of the overall cross-correlation (at about $-8$ and $+6$ months; see Fig. 4a) towards shorter lag/lead times (as seen in Fig. 4a). The changes in coupling of $h$ to T ($a_{21}$), in turn, contribute very little to the changes in the cross-correlation.

### 3.5 Sensitivity of ENSO predictability to the changes in the dynamics

The changes of the ENSO dynamics we described above have the potential to affect the predictability of ENSO. The CMIP5 simulations do not give any indication of predictability of ENSO or changes thereof, as the ensemble does not include forecast runs. We can use the ReOsc model integrations to approximate the predictability of ENSO in the CMIP5 simulations based on the model parameters and changes thereof. This, however, should only be considered with some caution, as it does not fully reflect the dynamics and predictability of ENSO in the CMIP models. Thus, it is an outlook to motivate further studies on change in the predictability of ENSO. Again, we will focus on the *Z20* estimates and do not discuss the *maxgrad* estimates, as they are qualitatively similar but weaker.

We conduct a long ReOsc model control integration with the mean model parameters from the CMIP5 historical simulations. We then start forecast runs at 400 different initial conditions from the control run, each being 5 years apart from each other. In the forecast runs the noise forcings of the ReOsc model is chosen to be different from the control run, creating a new independent realization of the $T$ to $h$ evolution. The forecast skill is evaluated by the correlation between the control and forecast run at different lead times, see Fig. 10a. We repeat these simulations with the same noise values, but with the mean model parameters from the CMIP5 RCP8.5 simulations (Fig. 10a). The difference in the forecast correlation skill between the historical and the RCP8.5 simulation result purely from the difference in the model parameters. Since the noise forcings are identical in these runs there are no statistical uncertainties in the differences between the runs resulting from the random noise.

We can first of all note that the correlation skill scores of the CMIP5 historical runs are decreasing relatively fast, if

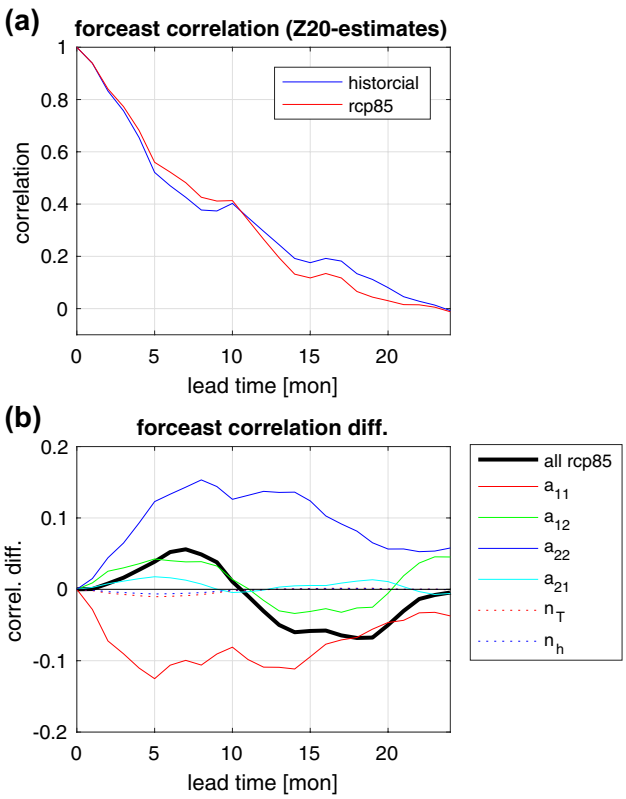


**Fig. 10** **a** Anomaly correlation skill in the ReOsc forecast integrations for historical (blue) and RCP8.5 (red) CMIP ensemble mean model parameters. **b** Changes in the correlation skill in the ReOsc forecast integrations due to changes in the individual ReOsc parameters. See text for details

compared to published ENSO forecast skills (Jin et al. 2008). This mostly reflects the limited skill of the ReOsc model, but does not suggest that the CMIP5 have lower ENSO predictability than state-of-the-art forecast models. We therefore have to take these results with a grain of caution, as the true ENSO predictability in the CMIP5 model simulations is likely to be significantly larger than presented in these ReOsc model runs.

The RCP8.5 runs show a clear change in forecast correlation skill relative to the historical run, with larger forecast skill for shorter (< 10 months) lead times and smaller forecast skill for longer lead times (Fig. 10a, b). We can evaluate the sensitivity of these changes in the forecast skills to the individual ReOsc model parameters by repeating these simulations with the same noise values, but with the mean model parameters from the CMIP5 historical simulations and a single parameter from the RCP8.5 simulations (Fig. 10b).

The changes in the parameters $a_{11}$ and $a_{22}$ have the largest impact on the predictability. The increased damping of $T$ ($a_{11}$) results into decreased forecast correlation skill on all lead times. In turn, the decreased damping of $h$ ($a_{22}$) results into increased forecast correlation skill on all lead times, mostly compensating the changes from $a_{11}$. The changes in the coupling of $T$ to $h$ ($a_{12}$) most closely follow the overall change in the correlation skill (Fig. 10b), suggesting that they contribute significantly to the overall shift in forecast skill.

## 4 Summary and discussion

In this study, we analysed the changes in the linear ReOsc model dynamics, as they are simulated in CMIP5 simulations for the RCP8.5 scenario relative to the historical control simulation. The primary focus in this study was on the growth rate of $T$ and $h$, the coupling between the two and the noise forcing driving the ENSO variability. We further focused on the feedbacks controlling the growth rate of $T$, namely the Bjerknes wind-SST, the atmospheric net heat flux and the residual oceanic feedback. The CMIP5 ensemble shows fairly significant changes in nearly all of these important elements of the ENSO dynamics, despite the fact that the ensemble shows very little changes in the overall ENSO variability strength or periodicity (time scale behaviour of the power spectrum).

The growth rate of $T$ weakens in nearly all simulations, reflecting more strongly damped ENSO dynamics. This results from a combination of changes in the main feedbacks. The atmospheric net heat flux feedbacks become more strongly damped in all simulations, supporting the overall decrease in growth rate of $T$. However, this is overcompensated by an increased Bjerknes wind-SST in most simulations. The increased Bjerknes feedback leads to an increased growth rate of $T$, which in combination with the also increased negative net heat flux feedbacks still leads to an overall atmospheric growth rate change that is positive. The residual oceanic feedbacks are becoming more negative and therefore lead to the overall decrease in growth rate of $T$.

Other notable changes in the ENSO dynamics are an increase in the growth rate of $h$ in most simulations, leading to a less damped $h$ variability. The coupling of $T$ to $h$ is also increasing in most simulations, reflecting a $T$ variability that is more strongly influenced by variation in $h$. In turn, the coupling of $h$ to $T$ is becoming weaker (less negative), indicating that $h$ becomes slightly less sensitive to $T$. The strength in noise forcings on $T$ or $h$ shows little to no changes.

The ReOsc model framework allows us to estimate the sensitivity of ENSO variability to these dynamical changes. It can also explain why there is essentially no changes in ENSO variability, while there are significant changes in the ENSO dynamics. The strength of the ENSO variability ($T$) is not changing due to compensating effects of the decrease in growth rate of $T$ that is concurrent with an increase in growth rate of $h$. Similarly, the periodicity or time scale behaviour of ENSO is not changing due to compensating effects. The decreases in the growth rates of $T$ alone, would reduce the interannual ENSO oscillations, which would be reflected in an increase in the spectral slope (slope flattens). This is, however, compensated by the increase in the growth rates of $h$ and by the increased coupling of $T$ to $h$, leading effectively to no changes in spectral slope.

It is difficult to compare these findings in changes of ENSO dynamics with previous studies based on the BJ-index stability or SST heat budget analysis, due to the inherently different approaches taken and due to the different set of models analysed (Kim and Jin 2011; Chen et al. 2015). However, we think that there is some agreement between these studies. Reported changes in atmospheric feedbacks ($c_{fT}$ and $c_{\tau T}$) and mean thermocline depth are largely consistent. Compensating effects in different dynamics leading to no overall changes in stability found in Kim and Jin (2011) appears to be consistent with our findings. Further studies should, however, combine the ReOsc modelling approach with the BJ-index stability analysis to gain better understanding of the process controlling the ENSO dynamics in a changing climate.

While the above described dynamical changes may effectively not change the overall ENSO variability statistics, they can potentially affect the predictability of ENSO. The CMIP5 ensemble does not allow to directly evaluate the predictability of ENSO, but the ReOsc model framework can be used to get some approximation of predictability changes in the CMIP5 simulations. The ReOsc model analysis indicates that the predictability of ENSO increases for shorter lead times (< 9 months), but decreases on longer lead times. This

is due to reduced predictability by the decreased growth rate of $T$, and an increased predictability due to the increased growth rate of $h$. The shift towards higher predictability at shorter lead times and lower predictability longer lead times is linked to the increased coupling strength of $T$ to $h$. This is also reflected in the changes in cross-correlation between $T$ and $h$, which shifts to shorter lead times when $h$ leads $T$. However, we have to keep in mind that we used the ReOsc model as surrogate model of the CMIP simulations. Further, more in-depth studies using CMIP models are required to address the predictability changes in more detail.

The CMIP5 ensemble also shows significant changes in the mean thermocline depth, which are likely to contribute to the dynamical changes found. Here it does matter whether thermocline depth is estimated by *Z20* isotherm or by *maxgrad*. The latter should be more appropriate for climate change studies, as it is not affected by the mean temperature of the profile, but it does reflect the 'true' thermocline depth. The changes in temperature profile show a remarkable minimum change at the depth that coincides with the historical mean thermocline depth. This suggest a significant dynamical adjustment of the upper equatorial Pacific that is not just a reflection of a transient warming with more warming at the surface and less warming in deeper layers.

It is beyond the scope of this study to fully analysis why we observe the dynamical changes described above. However, some indications may be given from the analysis presented here. The increased negative net heat flux feedback and the increased positive Bjerknes feedback are both likely to be related to the El Niño like mean state changes. At least this would be consistent with some previous findings: first it was shown before that the CMIP5 ensemble has a mean cold tongue bias in the SST and too weak net heat flux and positive Bjerknes feedback (Bellenger et al. 2014; VB18). It was further shown that these two feedbacks are indeed related to the mean sst biases (Lloyd et al. 2012; Bayr et al. 2018). If we further consider that the CMIP5 ensemble has an El Niño like mean state changes in the RCP8.5 scenario (Collins et al. 2010; Liu et al. 2005), then the mean SST in the RCP8.5 scenarios is effectively reducing the CMIP5 ensemble mean state cold tongue biases. Subsequently, the negative net heat flux and the positive Bjerknes feedback are both expected to increase too.

The increase in the growth rate of the thermocline, the reduced overall variability of $h$ and the changes in the coupling between $T$ and $h$ is likely to partly result from the shallower mean thermocline depth with a sharper temperature gradient in the RCP8.5 scenario. Since thermocline depth is a positive definite number, it is likely that its variability is proportional to its mean value, if no other dynamical changes occur. Thus, a shallower mean $h$ would go along with a reduced variability of $h$. The sharper temperature profile in the RCP scenario can potentially support less damped variability of $h$, and therefore supports an increased growth rate. However, the picture is more complex with different behaviours in the mean *Z20* and *maxgrad* estimates, with additional different regional changes and other dynamical changes occurring.

The linear ReOsc model approach presented here, neglects non-linearities in the ENSO dynamics and therefore cannot make any statements on how non-linear ENSO dynamics may change in the future climate change. It further also does not consider regional shifts in ENSO, such as shifts towards more east or central Pacific events. However, non-linear dynamics or regional patterns of ENSO are important aspects of ENSO dynamics and studies have shown that they can potentially change (Yeh et al. 2009; Boucharel et al. 2011; Cai et al. 2015a). It is therefore interesting to see how this ReOsc modelling approach could be used to address such problems. This will be addressed in future studies.

Finally, we have to give some caveat note about this CMIP5 ensemble result.

Although, we find highly significant changes in the dynamics of ENSO in the CMIP5 ensemble this does not necessarily imply that the real world will respond in the same way. The CMIP5 ensemble has substantial common biases in the ENSO dynamics discussed here and in its mean state (Bellenger et al. 2014; VB18). Furthermore, the CMIP5 ensemble does have a significant spread in its mean state, the mean ENSO dynamics and how it responses in the RCP8.5 scenario. Combined, these common model biases and spread undermine the reliability of these results. It also illustrates that ENSO in a climate system with slightly different mean states and slightly different mean ENSO dynamics, as simulated in individual CMIP5 models, can respond differently to climate change. It thus requires better understanding of the underlying processes and resolving the common model bias issues to gain more confidence about future changes in ENSO dynamics.

**Acknowledgements** The work was supported by the Australian Research Council (ARC) Centre of Excellence in Climate System Science (CE110001028), the ARC Centre of Excellence in Climate Extremes (CE170100023) and the ARC project "Beyond the linear dynamics of the El Niño Southern Oscillation" (DP120101442). The work presented here has a long history going back to 2007 with a number of people contributing to the analysis over time that we like to acknowledge here: Malte Jansen, Claudia Frauen, Simona Trefalt, Chevillard Jeanne and Payan Timothée and Yanshan Yu.

## References

Bayr T, Dommenget D, Martin T, Power SB (2014) The eastward shift of the Walker circulation in response to global warming and its relationship to ENSO variability. Clim Dyn 43:2747–2763. https://doi.org/10.1007/s00382-014-2091-y

Bayr T, Latif M, Dommenget D, Wengel C, Harlaß J, Park W (2018) Mean-state dependence of ENSO atmospheric feedbacks in climate models. Clim. Dyn. 50:3171–3194. https://doi.org/10.1007/s00382-017-3799-2

Bellenger H, Guilyardi E, Leloup J, Lengaigne M, Vialard J (2014) ENSO representation in climate models: from CMIP3 to CMIP5. Clim Dyn 42:1999–2018. https://doi.org/10.1007/s00382-013-1783-z

Boucharel J, Dewitte B, du Penhoat Y, Garel B, Yeh S-W, Kug J-S (2011) ENSO nonlinearity in a warming climate. Clim Dyn 37:2045–2065

Burgers G, Jin FF, van Oldenborgh GJ (2005) The simplest ENSO recharge oscillator. Geophys Res Lett 32:1–4. https://doi.org/10.1029/2005GL022951

Cai W, Wang G, Santoso A, McPhaden MJ, Wu L, Jin FF, Timmermann A, Collins M, Vecchi G, Lengaigne M, England MH, Dommenget D, Takahashi K, Guilyardi E (2015a) Increased frequency of extreme La Niña events under greenhouse warming. Nat Clim Change 5(2):132–137

Cai W et al (2015b) ENSO and greenhouse warming. Nat Clim Change 5:849–859. https://doi.org/10.1038/nclimate2743

Capotondi A, Sardeshmukh PD (2017) Is El Niño really changing? Geophys Res Lett 44:8548–8556. https://doi.org/10.1002/2017GL074515

Chen L, Li T, Yu Y (2015) Causes of strengthening and weakening of ENSO amplitude under global warming in four CMIP5 models. J Clim 28:3250–3274

Chen C, Cane MA, Wittenberg AT, Chen D (2017) ENSO in the CMIP5 simulations: life cycles, diversity, and responses to climate change. J Clim 30:775–801. https://doi.org/10.1175/jcli-d-15-0901.1

Collins M et al (2010) The impact of global warming on the tropical Pacific Ocean and El Niño. Nat Geosci 3:391–397. https://doi.org/10.1038/ngeo868

Dinezio PN, Kirtman BP, Clement AC, Lee SK, Vecchi GA, Wittenberg A (2012) Mean climate controls on the simulated response of ENSO to increasing greenhouse gases. J Clim 25:7399–7420. https://doi.org/10.1175/JCLI-D-11-00494.1

England MH et al (2014) Recent intensification of wind-driven circulation in the Pacific and the ongoing warming hiatus. Nat Clim Change 4:222–227. https://doi.org/10.1038/nclimate2106

Frauen C, Dommenget D (2010) El Niño and la Niña amplitude asymmetry caused by atmospheric feedbacks. Geophys Res Lett 37:1–6. https://doi.org/10.1029/2010GL044444

Guan C, McPhaden MJ (2016) Ocean processes affecting the twenty-first-century shift in ENSO SST variability. J Clim 29:6861–6879. https://doi.org/10.1175/JCLI-D-15-0870.1

Jansen MF, Dommenget D, Keenlyside N (2009) Tropical atmosphere–ocean interactions in a conceptual framework. J Clim 22:550–567. https://doi.org/10.1175/2008JCLI2243.1

Jin F-F (1997) An equatorial ocean recharge paradigm for ENSO. Part II: a stripped-down coupled model. J Atmos Sci 54:830–847. https://doi.org/10.1175/1520-0469(1997)054%3c0830:aeorpf%3e2.0.co;2

Jin FF, Kim ST, Bejarano L (2006) A coupled-stability index for ENSO. Geophys Res Lett 33:L23708

Jin EK et al (2008) Current status of ENSO prediction skill in coupled ocean–atmosphere models. Clim Dyn 31:647–664. https://doi.org/10.1007/s00382-008-0397-3

Kessler WS (1990) Observations of long Rossby waves in the northern tropical Pacific. J Geophys Res. https://doi.org/10.1029/jc095ic04p05183

Kim ST, Jin FF (2011) An ENSO stability analysis. Part II: results from the twentieth and twenty-first century simulations of the CMIP3 models. Clim Dyn 36:1609

Kim ST, Cai W, Jin FF et al (2014) ENSO stability in coupled climate models and its association with mean state. Clim Dyn 42:3313

Kohyama T, Hartmann DL, Battisti DS (2017) La Niña-like mean-state response to global warming and potential oceanic roles. J Clim 30:4207–4225. https://doi.org/10.1175/JCLI-D-16-0441.1

Lee T, McPhaden MJ (2010) Increasing intensity of El Niño in the central-equatorial Pacific. Geophys Res Lett 37:1–5. https://doi.org/10.1029/2010GL044007

Liu Z, Vavrus S, He F, Wen N, Zhong Y (2005) Rethinking tropical ocean response to global warming: the enhanced equatorial warming. J Clim. https://doi.org/10.1175/jcli3579.1

Lloyd J, Guilyardi E, Weller H (2012) The role of atmosphere feedbacks during ENSO in the CMIP3 models. Part III: the shortwave flux feedback. J Clim 25:4275–4293. https://doi.org/10.1175/JCLI-D-11-00178.1

Lübbecke JF, Mcphaden MJ (2014) Assessing the twenty-first-century shift in enso variability in terms of the bjerknes stability index. J Clim 27:2577–2587. https://doi.org/10.1175/JCLI-D-13-00438.1

Luo Y, Lu J, Liu F, Liu W (2015) Understanding the El Niño-like oceanic response in the tropical Pacific to global warming. Clim Dyn 45:1945–1964. https://doi.org/10.1007/s00382-014-2448-2

Luo Y, Lu J, Liu F, Garuba O (2017) The role of ocean dynamical thermostat in delaying the El Niño-Like response over the equatorial Pacific to climate warming. J Clim 30:2811–2827. https://doi.org/10.1175/jcli-d-16-0454.1

Luo JJ, Wang G, Dommenget D (2018) May common model biases reduce CMIP5's ability to simulate the recent Pacific La Niña-like cooling? Clim Dyn 50:1335–1351. https://doi.org/10.1007/s00382-017-3688-8

Maher N, Sen Gupta A, England MH (2014) Drivers of decadal hiatus periods in the 20th and 21st centuries. Geophys Res Lett 41:5978–5986

Manabe S, Stouffer RJ, Spelman MJ, Bryan K (1991) Transient responses of a coupled ocean–atmosphere model to gradual changes of atmospheric $CO_2$. Part I. Annual mean response. J Clim 4:785–818

McPhaden MJ (2012) A 21st century shift in the relationship between ENSO SST and warm water volume anomalies. Geophys Res Lett 39:1–5. https://doi.org/10.1029/2012GL051826

McPhaden MJ, Lee T, McClurg D (2011) El Niño and its relationship to changing background conditions in the tropical Pacific Ocean. Geophys Res Lett 38:2–5. https://doi.org/10.1029/2011GL048275

Meyers G (1979) On the annual Rossby wave in the tropical north Pacific ocean. J Phys Oceanogr. https://doi.org/10.1175/1520-0485(1979)009%3c0663:otarwi%3e2.0.co;2

Moss RH et al (2010) The next generation of scenarios for climate change research and assessment. Nature 463:747–756. https://doi.org/10.1038/nature08823

Rhein M, Rintoul SR, Aoki S, Campos E, Chambers D, Feely RA, Gulev S, Johnson GC, Josey SA, Kostianoy A, Mauritzen C, Roemmich D, Talley LD, Wang F (2013) Observations: ocean. In: Stocker TF, Qin D, Plattner G-K, Tignor M, Allen SK, Boschung J, Nauels A, Xia Y, Bex V, Midgley PM (eds) Climate change 2013: the physical science basis. Contribution of working group I to the fifth assessment report of the intergovernmental panel on climate change. Cambridge University Press, Cambridge

Smith NR (1995) An improved system for tropical ocean subsurface temperature analyses. J Atmos Ocean Technol 12(4):850–870. https://doi.org/10.1175/1520-0426(1995)012%3c0850:AISFTO%3e2.0.CO;2

Stevenson S, Fox-Kemper B, Jochum M, Neale R, Deser C, Meehl G (2012) Will there be a significant change to El Niño in the twenty-first century? J Clim. https://doi.org/10.1175/jcli-d-11-00252.1

Taylor KE, Stouffer RJ, Meehl GA (2012) An overview of CMIP5 and the experiment design. Bull Am Meteorol Soc 93:485–498. https://doi.org/10.1175/BAMS-D-11-00094.1

Van Oldenborgh GJ, Philip S, Collins M (2005) El Niño in a changing climate: a multi-model study. Ocean Sci 1:81–95

Vecchi GA, Soden BJ (2007) Global warming and the weakening of the tropical circulation. J Clim 20:4316–4340. https://doi.org/10.1175/JCLI4258.1

Vecchi GA, Soden BJ, Wittenberg AT, Held IM, Leetmaa A, Harrison MJ (2006) Weakening of tropical Pacific atmospheric circulation due to anthropogenic forcing. Nature 1:1. https://doi.org/10.1038/nature04744

Vijayeta A, Dommenget D (2017) An evaluation of ENSO dynamics in CMIP simulations in the framework of the recharge oscillator model. Clim Dyn. https://doi.org/10.1007/s00382-017-3981-6

Wittenberg AT, Rosati A, Delworth TL, Vecchi GA, Zeng F (2014) ENSO modulation: is it decadally predictable? J Clim 27:2667–2681

Yang H, Wang F (2009) Revisiting the thermocline depth in the equatorial Pacific. J Clim 22:3856–3863. https://doi.org/10.1175/2009JCLI2836.1

Yeh SW, Kug JS, Dewitte B, Kwon MH, Kirtman BP, Jin FF (2009) El Nĩo in a changing climate. Nature 461:511–514. https://doi.org/10.1038/nature08316

Yoshimori M, Watanabe M, Shiogama H, Oka A, Abe-Ouchi A, Ohgaito R, Kamae Y (2016) A review of progress towards understanding the transient global mean surface temperature response to radiative perturbation. Prog Earth Planet Sci 3:21

Zhao M, Hendon HH, Alves O, Liu G, Wang G (2016) Weakened Eastern Pacific El Nino predictability in the early twenty-first century. J Clim 29:6805–6822. https://doi.org/10.1175/JCLI-D-15-0876.1